



EUROfusion

WPPFC-CPR(18) 18866

K Heinola et al.

Modelling of the effect of ELMs on fuel recycling at JET-ILW divertor target

Preprint of Paper to be submitted for publication in Proceeding of 23rd International Conference on Plasma Surface Interactions in Controlled Fusion Devices (PSI-23)



This work has been carried out within the framework of the EUROfusion Consortium and has received funding from the Euratom research and training programme 2014-2018 under grant agreement No 633053. The views and opinions expressed herein do not necessarily reflect those of the European Commission.

This document is intended for publication in the open literature. It is made available on the clear understanding that it may not be further circulated and extracts or references may not be published prior to publication of the original when applicable, or without the consent of the Publications Officer, EUROfusion Programme Management Unit, Culham Science Centre, Abingdon, Oxon, OX14 3DB, UK or e-mail Publications.Officer@euro-fusion.org

Enquiries about Copyright and reproduction should be addressed to the Publications Officer, EUROfusion Programme Management Unit, Culham Science Centre, Abingdon, Oxon, OX14 3DB, UK or e-mail Publications.Officer@euro-fusion.org

The contents of this preprint and all other EUROfusion Preprints, Reports and Conference Papers are available to view online free at <http://www.euro-fusionscipub.org>. This site has full search facilities and e-mail alert options. In the JET specific papers the diagrams contained within the PDFs on this site are hyperlinked

Modelling of the effect of ELMs on fuel recycling at the bulk W divertor of JET

K. Heinola^{1,2*}, T. Ahlgren¹, S. Brezinsek³, T. Vuoriheimo¹ S. Wiesen³ and JET Contributors[†]

¹*Department of Physics, University of Helsinki,
P.O. Box 64, 00560 Helsinki, Finland*

²*International Atomic Energy Agency IAEA, A-1400 Vienna, Austria and*

³*Forschungszentrum Julich GmbH, D-52425, Julich, Germany*

Abstract

Effect of ELMs on fuel retention at the bulk W target of JET ITER-Like Wall was studied with multi-scale calculations. Plasma input parameters were taken from ELMy H-mode plasma experiment. The energetic intra-ELM fuel particles get implanted and create near-surface defects up to depths of few tens of nm, which act as the main fuel trapping sites during ELMs. Clustering of implantation-induced vacancies were found to take place. The incoming flux of inter-ELM plasma particles increases the different filling levels of trapped fuel in defects. The temperature increase of the W target during the pulse increases the fuel detrapping rate. The inter-ELM fuel particle flux refills the partially emptied trapping sites and fills new sites. This leads to a competing effect on the retention and release rates of the implanted particles. At high temperatures the main retention appeared in larger vacancy clusters due to increased clustering rate.

PACS numbers: 28.52.Fa 52.55.Fa 52.55.Pi 52.70.Nc 52.77.Dq

* Corresponding author *Email:* `kalle.heinola@helsinki.fi`

[†] See the author list of X. Litaudon et al. Nucl. Fusion 57, 102001 (2017)

I. INTRODUCTION

The JET tokamak with its ITER-Like Wall (ILW) project [1] provides a unique opportunity to study the plasma-material interactions (PMI), such as erosion, deposition, and fuel retention taking place in operating the next-step fusion device ITER. The ILW plasma-facing components (PFCs) comprise of main chamber limiters made of bulk beryllium (Be) and of divertor armour tiles either made of bulk tungsten (W), or W-coated carbon-fibre composite (CFC) tiles. The understanding and control of the PMIs, such as short-term [2] and long-term [3, 4] fuel retention, and migration and deposition of the eroded wall material [4–9] are of vital importance for economical operation of a future fusion reactor.

The post-mortem analyses of the JET-ILW PFCs retrieved from the JET vessel after the first operational ILW campaign 2011-2012 mapped the global distribution of the deposits and fuel retention inside the machine ([3, 5–7, 10, 11] and references therein). The global fuel retention rate was found to have decreased in JET-ILW by a factor > 18 as compared to operations with the previously installed all-carbon wall of JET (JET-C) [3]. Gas balance measurements performed during the first ILW campaign have shown a factor 10-20 reduction in the long-term fuel retention measurements as compared to JET-C [2]. A more detailed experimental study on the local fuel recycling at the JET-ILW plasma strike points showed the evolution and dynamics of near-surface retention, implantation, outgassing and retention of fuel on W being affected by the surface temperature evolution during the plasma loading [12]. In that work, using subsequent plasma discharge series for steady-state plasmas in L-mode the W target temperature was observed to increase from 65°C up to $\sim 350^{\circ}\text{C}$ owing to power deposition during plasma discharges (duration ~ 20 s) and only inertial cooling between subsequent discharges (~ 20 min between pulses). This temperature change resulted in decrease of the short-term fuel retention in W divertor by $1/3$ during the subsequent pulses. The effect of fast time-scale events on fuel retention in ILW W was studied with a series of identical H-mode plasmas with edge-localized modes (ELMs) [12]. The intra-ELM loads increase the particle and heat loads on the W target, and it was shown the ELM-induced temperature increase on the deposit-free bulk W target to exceed 1400°C at the end of the pulse.

Present work scrutinizes the ELM-induced effects on W target computationally with the concept of *multi-scale* calculations. Objective is in the local fuel retention and recycling

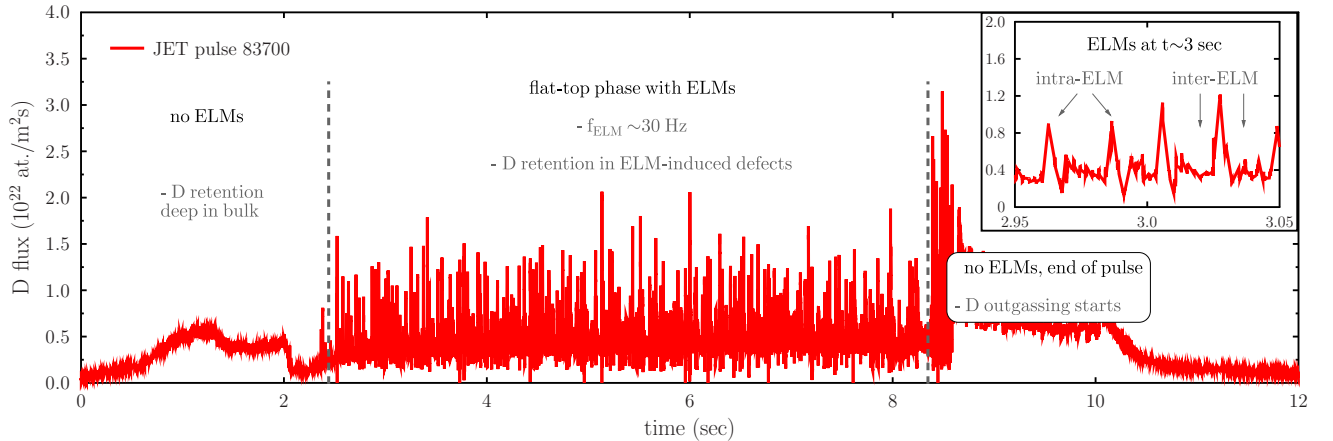


FIG. 1: The JET-ILW ELMy H-mode plasma pulse used in the RE calculations. D flux is measured with a Langmuir probe at the outer strike point on bulk W target where the outer strike line was kept static during the divertor phase of the discharge.

by studying computationally the bulk W divertor target properties during H-mode plasmas with type I ELMs. The method used solves numerically a set of rate theory equations (RE) describing the dynamics of the ELM-induced events and fuel retention occurring in the bulk and on the target surface [13, 14]. Equations are parametrised with first-principles calculations using electron density functional theories (DFT), with molecular dynamics (MD) simulations, and with binary collision approximation (BCA) calculations. The length and time scales in the present methodology can vary from \AA to meters, and from femtoseconds to minutes, respectively. The limitation of the present RE method is that the monitored concentrations (e.g. plasma particles, defects) are presented one-dimensionally as a function of depth, whereas there is no limitation in the number of particles, and the simulations can be executed with low computational cost. Thus, the method applied is presently the only computational approach suitable for simulating PMIs and ELM-induced defect dynamics and evolution on a fusion plasma-pulse scale by including the real physical processes taking place in the bulk of the target.

II. METHODOLOGIES

A. Fusion plasma experiment

Fuel recycling and dynamics at the W divertor target of JET-ILW has been studied with dedicated H-mode plasma experiments with type I ELMs in Ref. [12]. It was found that the resulted fuel content in the W target depends on the fuel particle impact energy and on the flux of the particles. Moreover, the dynamics is largely influenced by the temperature evolution of the target. In JET-ILW there is no active cooling of the PFCs, which results in large variation in the target temperature during plasma operations. The complex interplay of fuel retention, recycling, implantation, and outgassing can be investigated with various diagnostics of JET-ILW [15–18] via assessing the temperature evolution of the target, and the plasma particle fluxes, recycling, and impact energies at the target. The experiment comprised of 351 identical diverted ELMy H-mode pulses (JET pulse numbers (JPNs) 83623–83974 with auxiliary heating 11 MW and gas injection 10^{22} D s⁻¹), with the inner strike point on tile 3 (W-coated CFC) and the outer strike point (OSP) on tile 5 (bulk W). Pulse JPN83700 was chosen as a reference pulse for present work (Fig. 1).

An extensive analysis on the properties of the ELMs carried out in Ref. [12] showed the averaged D flux and energy to be $\sim 3.1 \times 10^{19}$ cm⁻²s⁻¹ and ~ 3 keV during an ELM (intra-ELM), respectively, and $\sim 1 \times 10^{19}$ cm⁻²s⁻¹ and 200 eV in-between ELMs (inter-ELM). The ELMs appeared on the flat-top phase of the pulse with a frequency $f_{\text{ELM}} \approx 30$ Hz (Fig. 1). The duration of the ELM footprint, characterized by the heat load pattern, on the W target is ~ 6 ms with a sharp rise of the D flux for 2 ms followed by a flux decay for $2 \text{ ms} < t < 6$ ms [12]. Integrating over the averaged ELM D flux profile one gets a D implantation dose of $(1.3 \pm 0.3) \times 10^{16}$ cm⁻² per single ELM. A fraction of this dose gets backscattered from the target surface due to the high mass difference between the projectile (D) and the the target (W) atoms, but the majority gets implanted in the target, and creates implantation-induced - or ELM-induced - defects in the bulk, such as mono-vacancies (V_1) and self-interstitials (I_1) [13]. The ELM-implanted D diffuses away from the implantation zone, or gets trapped to any of the defects in the bulk (ELM-induced defects, intrinsic defects and impurities, grain boundaries, etc). The out-diffused D can be seen as outgassing and desorption. Once the target temperature gets elevated during the pulse and subsequent ELMs, the thermodynamic

energy stored in the target increases the energy levels of the trapped particles inducing D release, which is seen as out-diffusion and fuel recycling at the target. In Ref. [19] it was noted the W target plate of JET-ILW representing an additional fuel particle sink for a few ms, which can be defined as required refill-time after an ELM crash. Understanding all these events taking place in the bulk of the target, requires examination at the atomic level. Hence, applying a modern multi-scale computational method provides atomistic level insight to the ELM-scale fuel retention events, and further, the same methodology can be extended covering all the ELM events taking place throughout the corresponding plasma pulse. In this work, the effect of ELMy H-mode plasma on D fuel retention on W target has been examined by using real experimental ILW plasma pulse data at the target as input for computations to study the trapping, release and recycling phenomena of fuel particles. In the following section, the computational methodology applied in this work is described and the formulation is given.

B. Computational method and simulation setup

The RE simulation method used is based on solving a set of rate equations describing all the physical and chemical processes in the target material. These include D plasma particle implantation, implantation-induced defect creation, diffusion of the plasma particles and defects, trapping to defects and to impurities carbon (C) and oxygen (O), release from and re-trapping to defects and impurities, diffusion of plasma particles and defects, and clustering and dissociation of defects or particle-defect systems. The RE method has been described in depth in Refs. [13, 14] and in the following only the main features are summarized. The concentration C for each examined distinct system, or entity - as function of depth and time - is given by the following coupled partial differential equations [20–22]:

$$\begin{aligned}
\frac{\partial C_\alpha(X, t)}{\partial t} = & D_\alpha \frac{\partial^2 C_\alpha(x, t)}{\partial x^2} \\
& + S_\alpha(x, t) \\
& \pm \sum_{\beta, \gamma=1}^N k_{\beta, \gamma}^2 D_\beta C_\beta(x, t) \\
& \pm \sum_{\delta=1}^N \nu_\delta \exp^{-\frac{E_{A, \delta}}{kT}} C_\delta(x, t),
\end{aligned} \tag{1}$$

where α , β , γ and δ stand for hydrogen, vacancy (V), self-interstitial atom (I), impurities (here C and O), and combinations of all of them. In total there are N distinct entities, which are monitored simultaneously.

The first term on the right-hand side of Eq. (1) is the diffusion of an entity α with a diffusion constant D_α . The second term S_α is the source, such as intra-ELM implantation of D and the corresponding creation of implantation-induced defects. Third term describes all the exothermic events, such as trapping of D and clustering of defects, with a corresponding sink strength, $k_{\beta,\gamma}^2$. The last term is for endothermic processes, such as detrapping of D and dissociation processes of defects described with a pre-exponential factor ν_δ , and an activation energy $E_{A,\delta}$ needed for the system δ to break up. DFT calculations were used in determining the fundamental properties of W, such as the bulk, surface, and the point defect properties of mono- and di-vacancies (V_1 and V_2), and interstitials (I_1) [23–26]. Further, DFT was used to determine the hydrogen properties in W - diffusion ($D_0 = 4.8 \times 10^{-8}$ m²/s and $E_m = 0.26$ eV) [25], and binding energies (E_b) to vacancies [24, 27] and to C and O impurities [14]. An assessment using the difference in the zero-point energies (ΔZPE) was applied for determining the energy needed for D to detrap from a defect as $E_t = E_b + E_m + \Delta ZPE$ (more details in Ref. [14]).

As described in Sect. II A, the simulation input parameters for the source term S were real ELMy H-mode plasma parameters at the OSP on the bulk W outer target plate of the ILW divertor. The D flux data as measured with a Langmuir probe on bulk W divertor tile 5, stack C, were taken as is without reducing the number of particles. The D impact energies were interpolated between the reported [12] averaged inter-ELM energy (200 eV/D) and the intra-ELM energy (3 keV/D). Resulted surface temperature evolution was calculated from the D flux (Fig. 2). The inter-ELM impact energy is not sufficient for creating any lattice damage due to the high displacement energy of W (90 eV [28]). In the calculations, all the lattice defects were created during intra-ELM impacts. The evolution of the ELM-induced defects (V_1 , I_1) was monitored in the simulations, and clustering of V_1 s up to V_2D_i ($i = 1 \dots 6$) was included.

Hydrogen traps easily to impurities in metals, which is often neglected in time-dependent simulations. The main impurity, excluding molybdenum, in a bulk W sample is C with concentration of ~ 10 $\mu\text{g/g}$ (typical high purity 99.99% polycrystalline W by Plansee AG), corresponding to about 10^{25} C at./m³. From this value a constant C concentration of 5×10^{18}

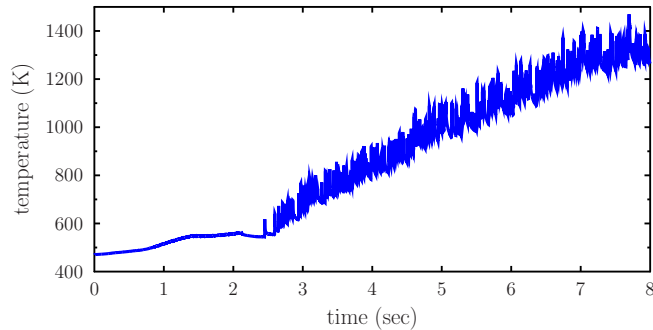


FIG. 2: Target temperature evolution as calculated from the D flux to the W target. At time > 2.4 s the temperature increases gradually, and the ELMs induce a pulsed increase to the temperature with $\Delta T \sim 100$ K reaching temperatures $\gtrsim 1400$ K in the end of the pulse.

cm^{-3} was chosen to be used in these calculations. Similarly, using real impurity values for O in W, a constant concentration of $2 \times 10^{18} \text{ cm}^{-3}$ was taken as O impurity level in the bulk W. Hydrogen trapping to grain boundaries were not included in this work. Also, clustering of vacancies to V_3, V_4, \dots and their effect to hydrogen trapping during ELMs will be part of a future work.

III. RESULTS

The D flux to the OSP (Fig. 1) shows two distinctive phases, or regions of the pulse. The time interval $0 < t < 2.4$ s, which has no ELMs, and the subsequent flat-top phase lasting for 6 s with ELMs. Further, the flat-top phase can be divided to intra-ELM and inter-ELM phases. During the plasma phase without ELMs, the impact energy of the incoming D is 200 eV per ion, which is high enough allowing the particles to penetrate the surface (if not backscattered), but not enough for creating any additional lattice damage in the bulk. However, the RE simulations show that the penetrated D particles do not stop in the bulk, but diffuse rapidly back to surface, or deeper in the bulk where they get trapped to the impurities C and O. After the first second of plasma exposure this trapped D profile is at depth $> 3 \mu\text{m}$, and reaches $7 \mu\text{m}$ at 2.4 s. The amount of free D on solute sites at 2.4 s is highest near the target surface $\sim 7 \times 10^{16} \text{ cm}^{-3}$, and the free D profile shows a decaying tail towards the bulk and goes to zero at $< 6 \mu\text{m}$.

The plasma flat-top phase including ELMs takes place after 2.4 s. The intra-ELM im-

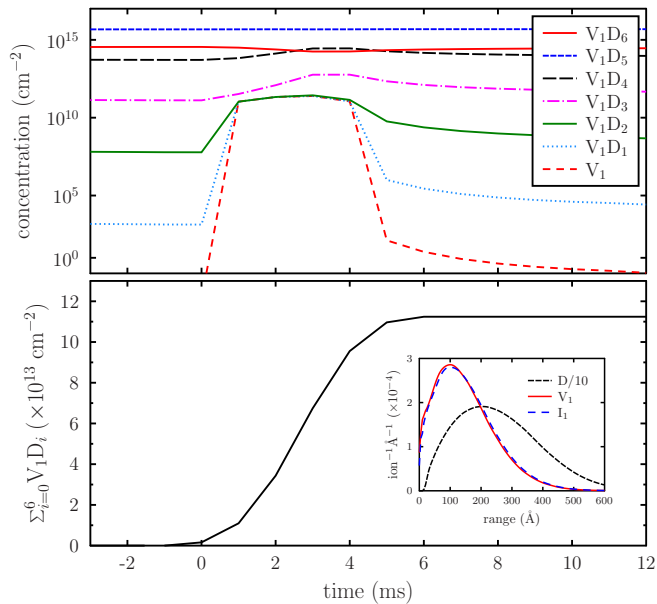


FIG. 3: (Color online) Top: Dynamics of vacancy creation, and trapping and release of D from vacancies during an ELM. A single ELM creates $\sim 10^{11}$ $1/\text{cm}^2$ new mono-vacancies (V_1), which together with the existing V_1 are filled with the incoming D particles. Beyond the ELM peak ($t > 6 - 7$ ms) the filling levels of V_1D_i entities ($i = 1 \dots 6$) get stabilized, and there are no empty V_1 left. Bottom: Evolution of all the D-filled V_1 during a single ELM. The amount of V_1D_i entities ($i = 1 \dots 6$) after an ELM is $\sim 10^{14}$ $1/\text{cm}^2$ (see text for details). The subfigure shows the ranges of ELM-implanted D with 3 keV, and the resulted defect (V_1 , I_1) distributions.

pact energy reaches 3 keV/D whereas the inter-ELM impact energies remain an order of magnitude lower at 200 eV/D. The intra-ELM energy is sufficient for creating implantation-induced damage in the target. In the RE calculations the defects created are the primary defects V_1 and I_1 , which were allowed to diffuse and trap D. As was calculated in Sect. II A a single ELM of duration ~ 6 ms on the average transports $(1.3 \pm 0.3) \times 10^{16}$ cm^{-2} of D to the target. The effect of this dose in the bulk is visualized in Fig. 3. The ELM creates approx. 10^{11} cm^{-2} new V_1 's instantaneously to near-surface region with a concentration profile maximum at ~ 10 nm. These defects get gradually filled during the first 2 ms by the incoming D. Also, the number of already existing V_1 's with different filling levels of D (V_1D_i ; $i = 1 \dots 6$), can be seen to increase during the ELM. By the end of the ELM ($2 \text{ ms} < t < 6 \text{ ms}$) as the incoming D flux decreases from its maximum value back to its background inter-ELM level and the temperature is increased due to heat absorption, the

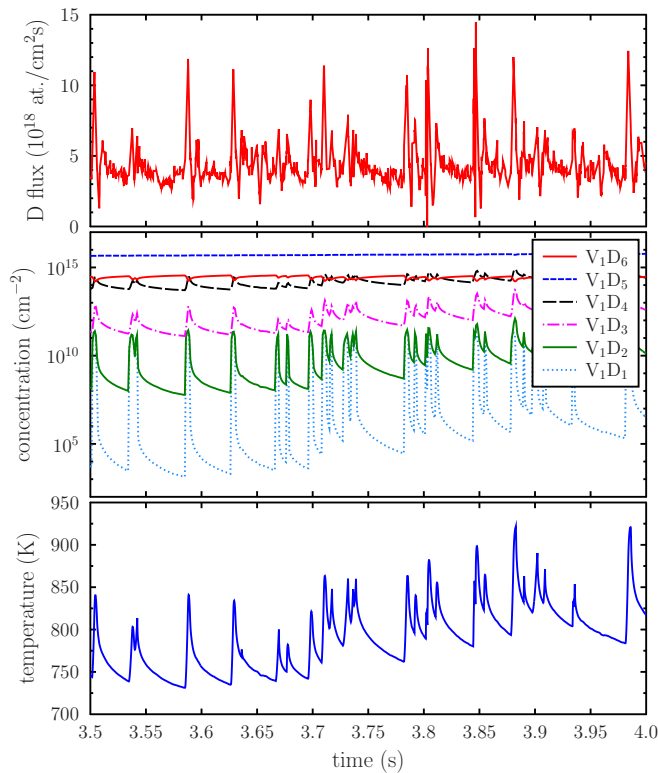


FIG. 4: (Color online) Example on the effect of multiple ELMs to bulk W target (time interval $3.5 \text{ s} < t < 4.0 \text{ s}$). Top: D flux as measured on the OSP. Centre: Dynamics of the V_1 filling levels due to retention, trapping and retrapping of D. Bottom: Temperature evolution at the OSP.

detrapping of D from V_1D_i 's takes place which is seen as a decrease in the D population of V_1 's. However, this detrapping flux is quickly balanced by the incoming inter-ELM flux of D, and the detrapping-retrapping processes appear to find an equilibrium during the inter-ELM phase. The time required for finding an equilibrium is $\sim 4 - 5 \text{ ms}$, which corresponds to the reported experimental refill-time at the OSP of JET-ILW [19]. As a result, the post-ELM retention in the target is higher by $\sim 10^{14} \text{ D cm}^{-2}$ compared to the pre-ELM retention. This complex intra-ELM filling and populating defects with D followed by emptying-filling processes during the inter-ELM phase takes place in the subsequent ELMs until the end of the pulse. A snapshot of the flat-top phase with longer timescale including multiple ELMs is shown in Fig. 4. Each ELM creates new vacancies which eventually increase the amount of retained D in the target by populating V_1 's with different filling levels of D. During the pulse the target temperature increases, which increases the D release rate from the defects, but which in turn competes with the retrapping rate and with the amount of new D coming

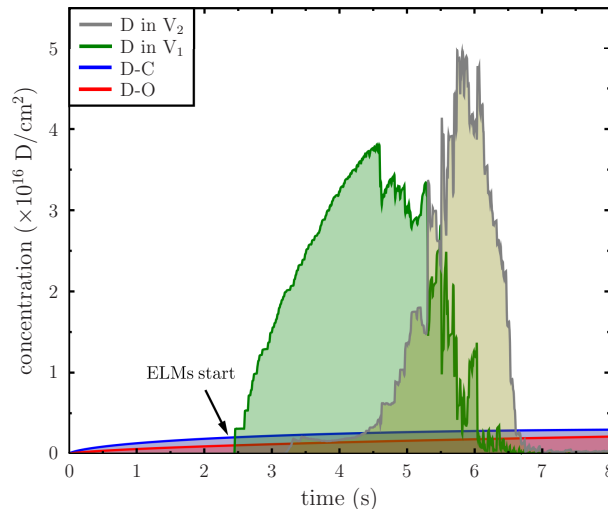


FIG. 5: (Color online) Effect of ELMs on the evolution of D trapping in and release from small vacancies (V_1 and V_2). Also shown the effect of C and O impurities to D trapping. As the temperature increases, the formation of V_2 s takes place as the V_1 s and V_1 s with D cluster. After the pulse only a fraction of D is retained in the V_1 and V_2 , whereas the impurities retain most of the D.

from the plasma into the bulk.

As the temperature keeps increasing the free V_1 become mobile and the clustering to V_2 is seen to take place via the reaction $V_1 + V_1D_i \rightarrow V_2D_i$ ($i = 1 \dots 6$). Clustering of V 's further into larger clusters (V_3, V_4, \dots) are part of a future work. Fig. 5 shows the formation and evolution of V_1D_i 's and V_2D_i 's during the pulse. Also is shown the evolution of D trapped to impurities C and O. The formation of V_1 's and V_2 's filled with different levels of D starts to take place as a direct influence of the ELMs. The number of V_1 's and V_2 's increase during the flat-top phase until the target temperature reaches level, where the diffusion of V_1 overrides the filling of V_1 with D. This can be seen at ~ 900 K ($t \sim 4.5$ s) as a sudden increase in the formation of V_2 accompanied with a corresponding decrease in the number of V_1 . This is a result of dynamical interplay between the creation of new V_1 's, D filling vacancies, and V_1 's becoming increasingly mobile resulting in abundance of V_2 's. However, as the target temperature increases even further to ~ 1100 K ($t \sim 6$ s), the D detrapping rate from V_2 propagates leaving more unfilled V_2 behind, which in turn face prompt dissociation at high temperatures [26]. In the end of the pulse there is only

a small fraction of D left in vacancies, whereas the majority of the retained D is trapped to the impurities C and O (Fig. 5). These concentration profiles of D trapped to C and O extend to several μm 's deep. In other words, the ELM-induced dynamical D retention and release events take place in the near-surface region of few tens of nm's, whereas the long-range and long-term D trapping extends deep in the bulk. This long-range trapping profile has been also observed experimentally in the post-mortem analyses (see e.g. Ref. [4] and references therein). However, the present calculations do not show the experimentally observed near-surface D concentration to remain after the pulse. Further calculations are required, and it may be that the near-surface D concentration originates from the ELM-induced effects where the trapped D is in large-sized vacancy-like clusters (V_3, V_4, \dots). Computational studies of ELM-induced defects including larger vacancy cluster sizes with hydrogen trapping properties are part of a future work.

IV. SUMMARY AND CONCLUSIONS

To summarize, plasma fuel retention at bulk W target during an ELMy H-mode pulse of JET-ILW has been studied computationally with multi-scale RE calculations. Real plasma parameters at the target, such as the D flux and impact energies, were used as input from a series of ELMy H-mode plasma experiments. D retention, diffusion, detrapping and re-trapping, ELM-induced defect creation, and intrinsic impurities in W were included in the calculations. Due to inertial cooling of JET-ILW the resulted temperature evolution plays a critical role in fuel retention and in the ELM-induced defect evolution. During an ELM, a complex interplay takes place between the defects created and the retention, detrapping and re-trapping of the incoming fuel particles. An averaged D implantation dose per ELM is $(1.3 \pm 0.3) \times 10^{16} \text{ cm}^{-2}$, which creates approximately 10^{11} cm^{-2} vacancies in the target. However, these vacancies get occupied with different filling levels of D in the ELM time scale. Moreover, as the temperature increases during the ELM, the formation of larger vacancy clusters, i.e. di-vacancies, takes place via mobilization and clustering of the mono-vacancies. The number of larger vacancy clusters and the amount of D trapped in the clusters increase during the pulse as the target temperature rises. At $\gtrsim 900 \text{ K}$ the number of D-filled mono-vacancies starts to vanish, whereas the formation of larger vacancy systems as D-filled di-vacancies keeps on increasing. This is the result of ELM-induced mono-vacancies becom-

ing highly mobile in ELM timescales due to the high target temperature. It has been shown in Ref. [26] the W di-vacancies having similar diffusion properties as the mono-vacancies, and that the dissociation probability of a di-vacancy increases exponentially with temperature. As a result of these properties, at temperatures $\gtrsim 1100$ K the amount of D-filled di-vacancies starts to decrease rapidly. The high temperature prevents the formation of new D-di-vacancy systems, since the diffusion of the ELM-induced vacancies becomes greater than the lifetime of the di-vacancy clusters. It is worth to highlight, the present work does not assess the formation of even larger vacancy clusters of V_3 , V_4 and so on. It has been shown in Ref. [13] the formation large-sized W vacancy clusters to take place in the near-surface region of couple of tens of nm during an ELM-relevant D implantation with few keV's in W. Further, in Refs. [23, 26] it was shown the large-sized vacancy clusters in W to be increasingly stable as the cluster size increases. Therefore, formation of large-sized vacancy clusters in W may take place during ELMs, and which can survive the high heats absorbed in the target during ELM pulses. Moreover, it is likely that these large-sized vacancy clusters trap fuel particles efficiently. The inner surfaces of the vacancy-type defects represent a surface-like trapping site for fuel particles. Thus, the high energy required for D surface-to-bulk motion in W [24] prevents the D of detrapping from large-sized vacancy-type defects even at very high temperatures. The effect of W main impurities C and O was seen to play a crucial role in D trapping. Even the typical levels of impurity concentrations may retain fuel particles at very high target temperatures. This is due to the impurity concentration profiles extending throughout the target providing a large trap reservoir for D. However, in the present work the assessment for D trapping to impurities was in its simplest form and no multiple filling levels were studied. Still one can conclude the impurities to play an important role in the long-term trapping due to the relatively high concentration levels. Another important factor affecting the fuel retention are the grain boundaries present in every polycrystalline material. Fuel trapping to W grain boundaries and the effect of grain boundary diffusion is part of a future work. As a final remark, the present studies on the effect ELMs at the target are connected to the plasma effects at the pedestal. The evolution of ELMs in time and the coupling of particle and heat transport in the pedestal in between ELMs are part of the pedestal model under development [29].

Acknowledgments

This work has been carried out within the framework of the EUROfusion Consortium and has received funding from the Euratom research and training programme 2014 – 2018 under grant agreement No 633053. The views and opinions expressed herein do not necessarily reflect those of the European Commission. Grants of computer time from the Center for Scientific Computing (CSC) in Espoo, Finland, and from University of Helsinki, Finland, are gratefully acknowledged.

- [1] G. F. Matthews, P. Edwards, T. Hirai, M. Kear, A. Lioure, P. Lomas, A. Loving, C. Lungu, H. Maier, P. Mertens, et al., *Phys. Scripta* **T128**, 137 (2007).
- [2] S. Brezinsek, T. Loarer, V. Philipps, H. Esser, S. Grünhagen, R. Smith, R. Felton, J. Banks, P. Belo, A. Boboc, et al., *Nucl. Fusion*. **53**, 083023 (2013).
- [3] K. Heinola, A. Widdowson, J. Likonen, E. Alves, A. Baron-Wiechec, N. Barradas, S. Brezinsek, N. Catarino, P. Coad, S. Koivuranta, et al., *Phys. Scripta* **T167**, 014075 (2016).
- [4] K. Heinola, A. Widdowson, J. Likonen, T. Ahlgren, E. Alves, C. F. Ayres, A. Baron-Wiechec, N. Barradas, S. Brezinsek, N. Catarino, et al., *Phys. Scripta* **2017**, 014063 (2017).
- [5] A. Widdowson, E. Alves, C. F. Ayres, A. Baron-Wiechec, S. Brezinsek, N. Catarino, J. P. Coad, K. Heinola, J. Likonen, G. F. Matthews, et al., *Phys. Scripta* **T159**, 014010 (2014).
- [6] J. P. Coad, E. Alves, N. P. Barradas, A. Baron-Wiechec, N. Catarino, K. Heinola, J. Likonen, M. Mayer, G. F. Matthews, P. Petersson, et al., *Phys. Scripta* **T159**, 014012 (2014).
- [7] M. Mayer, S. Krat, W. van Renterghem, A. Baron-Wiechec, S. Brezinsek, I. Bykov, P. Coad, Y. Gasparyan, K. Heinola, J. Likonen, et al., *ps* **T167** (2016).
- [8] M. Mayer, S. Krat, A. Baron-Wiechec, Y. Gasparyan, K. Heinola, S. Koivuranta, J. Likonen, C. Ruset, G. de Saint-Aubin, A. Widdowson, et al., *Phys. Scripta* **2017**, 014058 (2017).
- [9] J. W. Coenen, G. F. Matthews, K. Krieger, D. Iglesias, P. Bunting, Y. Corre, S. Silburn, I. Balboa, B. Bazylev, N. Conway, et al., *Phys. Scripta* **2017**, 014013 (2017).
- [10] J. Likonen, K. Heinola, A. D. Backer, S. Koivuranta, A. Hakola, C. F. Ayres, A. Baron-Wiechec, P. Coad, G. F. Matthews, and A. Widdowson, *Phys. Scripta* **T167**, 014074 (2016).
- [11] H. Bergsaker, I. Bykov, Y. Zhou, P. Petersson, G. Possnert, J. Likonen, S. Koivuranta, , and

- A. Widdowson, Phys. Scripta **T167** (2016).
- [12] S. Brezinsek, S. Wiesen, D. Harting, C. Guillemaut, A. J. Webster, K. Heinola, A. G. Meigs, M. Rack, Y. Gao, G. Sergienko, et al., Phys. Scripta **T167**, 014076 (2016).
- [13] T. Ahlgren, K. Heinola, K. Vörtler, and J. Keinonen, J. Nucl. Mater. **427**, 152 (2012).
- [14] K. Heinola and T. Ahlgren, J. Nucl. Mater. **438**, S1001 (2013).
- [15] I. Balboa, G. Arnoux, T. Eich, B. Sieglin, S. Devaux, W. Zeidner, C. Morlock, U. Kruezi, G. Sergienko, D. Kinna, et al., Rev. Sc. Instr. **83**, 10D530 (2012).
- [16] Ph.Mertens, H.Altmann, T.Hirai, V.Philipps, G.Pintsuk, J.Rapp, V.Riccardo, B.Schweer, I.Uytendhouwen, and U.Samm, J. Nucl. Mater. **390-391**, 967 (2009).
- [17] C. Guillemaut, A. Jardin, J. Horacek, A. Autricque, G. Arnoux, J. Boom, S. Brezinsek, J. W. Coenen, E. D. L. Luna, S. Devaux, et al., Plasma Phys. & Controlled Fusion **57**, 085006 (2015).
- [18] C. Guillemaut, A. Jardin, J. Horacek, I. Borodkina, A. Autricque, G. Arnoux, J. Boom, S. Brezinsek, J. W. Coenen, E. D. L. Luna, et al., Phys. Scripta **T167**, 014005 (2016).
- [19] S. Brezinsek, J. Nucl. Mater. **463**, 11 (2015).
- [20] A. McNabb and P. K. Foster, Trans. Metal. Soc. AIME **227**, 618 (1963).
- [21] M. I. Baskes and W. D. Wilson, Phys. Rev. B **27**, 2210 (1983).
- [22] S. M. Myers, P. Nordlander, F. Besenbacher, and J. K. Nørskov, Phil. Mag. A **48**, 397 (1983).
- [23] T. Ahlgren, K. Heinola, N. Juslin, and A. Kuronen, J. Appl. Phys. **107**, 033516 (2010).
- [24] K. Heinola and T. Ahlgren, Phys. Rev. B **81**, 073409 (2010).
- [25] K. Heinola and T. Ahlgren, J. Appl. Phys. **107**, 113531 (2010).
- [26] K. Heinola, F. Djurabekova, and T. Ahlgren, Nucl. Fusion. **58**, 026004 (2018).
- [27] K. Heinola, T. Ahlgren, K. Nordlund, and J. Keinonen, Phys. Rev. B **82**, 094102 (2010).
- [28] *Standard Practice for Neutron Radiation Damage Simulation by Charged-Particle Irradiation* (American Society for Testing and Materials, ASTM International, West Conshohocken, PA, 2009), ASTM E521 - 96 (2009).
- [29] S. Wiesen, M. Groth, M. Wischmeier, S. Brezinsek, A. Jarvinen, F. Reimold, and L. Aho-Mantila, Nuclear Materials and Energy **12**, 3 (2017).